

The effect of number of vacuum thermal evaporation cycles to the optoelectronic and morphological properties of ZnO

Fatin Farisha Alia Azmi¹, Saifful Kamaluddin Muzakir^{1*}, Mohd Fakhrul Zamani Kadir² and Shujahadeen B. Aziz^{3,4}

¹Material Technology Programme, Faculty of Industrial Sciences and Technology, Universiti Malaysia Pahang, Lebuhraya Tun Razak, Gambang, Kuantan, 26300, Pahang, Malaysia

²Center of Foundation Studies in Science, University of Malaya, 50603, Kuala Lumpur, Malaysia

³Advanced Polymeric Materials Research Lab, Department of Physics, College of Science, University of Sulaimani, Qylasan Street, Sulaimani, 46001, Kurdistan Regional Government, Iraq

⁴Department of Civil Engineering, College of Engineering, Komar University of Science and Technology, Sulaimani 46001, Kurdistan Regional Government, Iraq

Abstract

Zinc oxide (ZnO) is a wide band gap material (~3.37 eV) which has small exciton Bohr radius ~2.34 nm. In dye-sensitized solar cell, ZnO thin film is used as photoelectrode. Light-sensitive organic/ inorganic fluorophores could be adsorbed on the surface of the ZnO film, which later will be sandwiched with electrolyte and a counter electrode. The aim of this paper is to study the effect of number of evaporation cycle to the yielded morphology and size of ZnO building blocks; deposited using one, two, and three cycles of vacuum thermal evaporation technique. The ZnO thin films have been deposited on ITO glass substrate at vacuum pressure of 5×10^{-5} Torr, 116 A, and 2.6 V. The morphology of the thin films has been examined under Field Emission Scanning Electron Microscope (FESEM), which showed nanosphere morphology. The morphological observation is supported by a simulation; which calculated based on the crystallographic properties of the synthesized ZnO – characterized by X-ray diffractometer (XRD). Three sets of the ZnO thin films consists of ZnO particles in the range of 8 – 20 nm, 11 – 37 nm, and 6 – 16 nm respectively. According to the optical properties characterized by absorption spectrometer, it has been observed that the band gap of the thin films increased with increasing number of evaporation cycles. The values of the optical bandgap, E_g evaluated from Tauc's plot, were found in the range between 2.40 eV to 2.60 eV.

Keywords: nanostructures, thermal evaporator, zinc oxide

Article Info

Received 8th July 2020

Accepted 7th January 2021

Published 1st April 2021

*Corresponding author: Saifful Kamaluddin Muzakir; email: saifful@ump.edu.my

Copyright Malaysian Journal of Microscopy (2021). All rights reserved.

ISSN: 1823-7010, eISSN: 2600-7444

Introduction

Nanosized metal oxide semiconducting materials such as ZnO [1, 2], TiO₂ [3], Fe₂O₃ [4], and Ga₂O₃ [5], have attracted much attention, due to their unique ability to form various morphologies. Among them, ZnO was found to be a very promising candidate owing to its wide band gap (3.37 eV), and high exciton binding energy (~60 meV) at room temperature [6]. ZnO has been widely investigated for its catalytic [7], electrical [8], optoelectronic [9] and photochemical properties [10]. Low dimensional ZnO nanostructures such as nanospheres [11], nanoneedles [12], nanobelts [13], nanoribbons [14], nanoplate [15], and nanosheets [16] have attracted much attention for their potential applications in the fabrication of devices e.g., nanolaser [17], dye sensitized solar cells [18], photo catalyst [19], piezoelectric [20], and transparent light power electronics [21]. Figure 1 shows increment of publications from 1970 to 2019; generated from ISI Web of Science using keywords ‘ZnO’.

Furthermore, ZnO shows high electron mobility [22], electrical conductivity [23], and longer electron lifetime than that of the TiO₂; which indicates a possible significant reduction of unnecessary recombination of the injected excited state electrons from the main light absorber [24]. The dire need to conserve the energy of the excited state electron motivates researchers to explore the ZnO as photoelectrode, which would materialize a highly efficient excitonic solar cell.

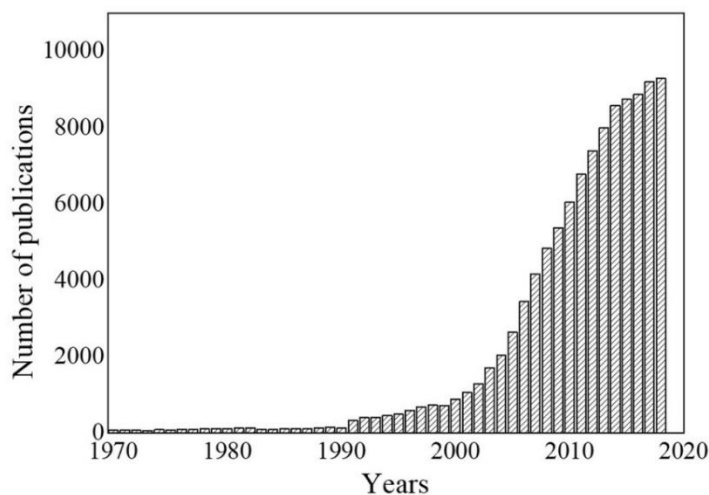


Figure 1: Number of papers published from 1970 to 2019; generated from ISI Web of Science using keywords ‘ZnO’.

Various techniques have been established to fabricate ZnO thin films, e.g., sol-gel [25], hydrothermal [26], spray deposition [27], thermal evaporation [28, 29], pulsed laser deposition [30], and chemical laser deposition [31]. Nevertheless, some of them have pitfalls such as long reaction time, toxic templates and poor crystallite quality of samples, which may affect the quality and applications of ZnO nanostructures [7]. Based on the previous study, the sol-gel method is commonly used due to low cost and simplicity [32-34]. However, the quality of the ZnO films fabricated using solution-based technique suffers from surface defects which act as trap states that favour unnecessary recombination of the excited state electrons [35, 36]. Herein, a vacuum thermal-evaporation procedure is employed in this study to achieve a high quality ZnO deposition, which has advantages of superior uniformity, smooth surface, thorough surface coverage, and accurate control of thickness [37]. Figure 2 shows an increasing trend of usage of vacuum thermal evaporator in various field from 2008 to 2020; indicates that this technique is gaining attention from researchers.

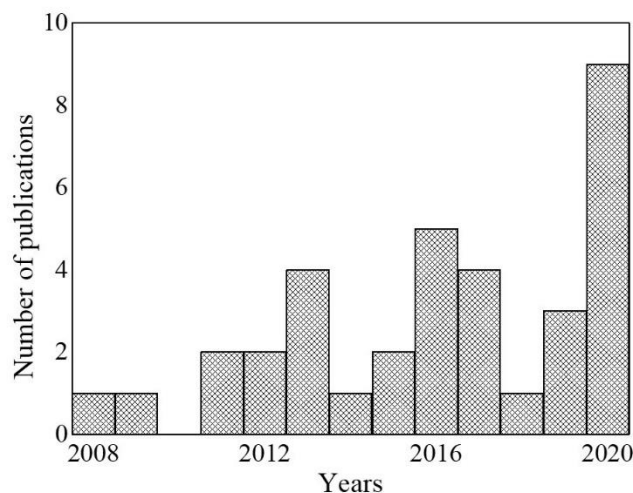


Figure 2: Number of papers published from 2008 to 2020; generated from ISI Web of Science using keywords ‘ZnO’ and ‘thermal evaporator’.

Enormous amount of study has been already reported on structure, optical and electrical properties of ZnO thin films. However, it still requires intensive research on fundamental properties of ZnO thin films. Hence, the objectives of the present work i.e., to study the effect of film thickness on; (i) crystal structure, (ii) morphology and (iii) optical properties of ZnO thin films using deposited using one, two, and three cycles of vacuum thermal evaporation technique. The thickness of the ZnO thin film would influence the photovoltaic conversion efficiency of a solar cell [38, 39], however, to the best of our knowledge, this fundamental study attracts less attention from researchers. Furthermore, the decrement of thickness of the bulk photoelectrode could contribute to i.e., (i) reduction of resistances, (ii) increment of electron lifetime, (iii) enhancement of electron separation, and (iv) enhancement of transportation of the electron and hole [40]. Keis et al. [41], Huang et al. [42], Shin et al. [43], Kao et al. [44], Xiao et al. [40], Bawvendi et al. [45], and Lan et al. [38] observed increment of device efficiency upon reduction of the thickness of the ZnO layer in solar cells. The crystal structure, morphological and optical properties of ZnO thin films were investigated by x-ray diffractometer (XRD), field emission electron microscope (FESEM), and ultraviolet–visible spectrophotometer.

Method and Materials

Preparation of materials

The ZnO thin films were deposited on ITO glass using thermal evaporator (Magna Value Thermal Evaporator; Model: TE MSSLAB/200). The ITO glass was cleaned with ethanol and distilled water before usage. The ZnO powder (0.040685 g) was carefully weighed and loaded into a molybdenum boat. The distance between the source and the substrate is ca. 5 cm (Figure 3). The pressure in the evaporator was maintained ca. 5×10^{-5} Torr, voltage of 2.6 V, and current of 116 A. The thin films were deposited under three conditions: (i) one, (ii) two and (iii) three evaporation cycles.

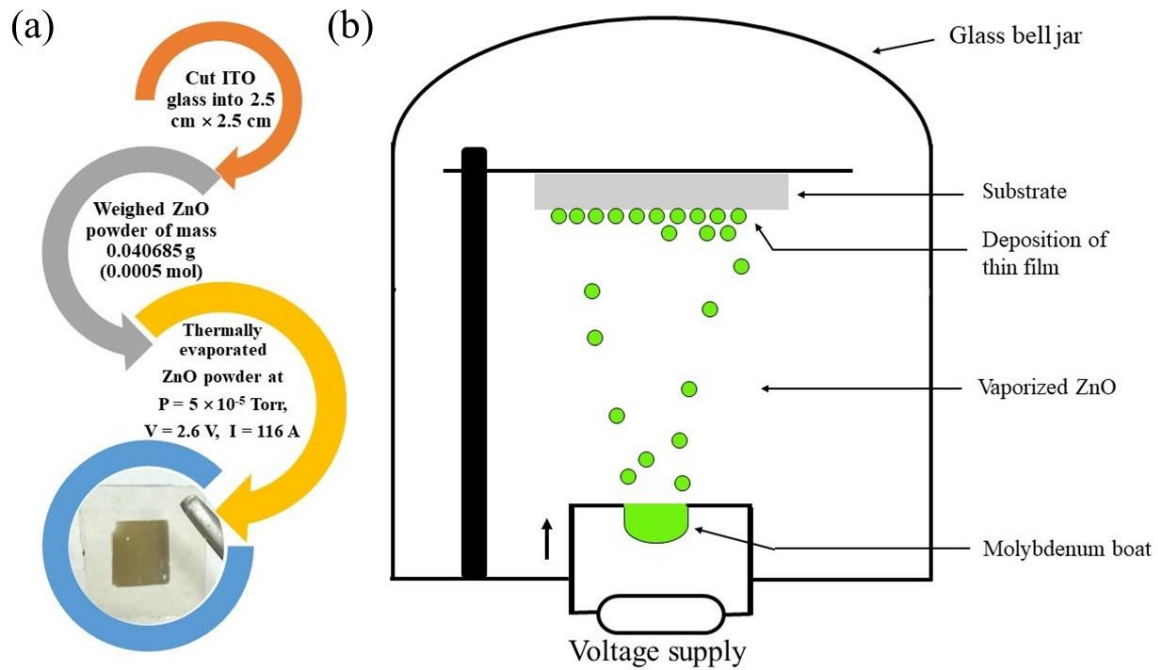


Figure 3: (a) ZnO thin film preparation scheme, and (b) Schematic diagram of thermal evaporator system

Material characterizations

The crystal structure of ZnO thin films was investigated using X-ray diffractometer (XRD) with Cu K α radiations (Rigaku Miniflex II). The surface morphology, and atomic fraction were examined using FESEM (Jeol JSM-7800F), and Energy Dispersive X-ray (EDX) spectrometer respectively. The ultraviolet-visible spectrophotometer (Shimadzu UV-2600) was used to characterize the optical properties of the ZnO thin films.

Results and Discussion

Crystal structure studies

The elemental compositions of the thin films fabricated using (i) one, (ii) two, and (iii) three evaporation cycles were examined using EDX spectroscopy; indicated in the insets of Figure 4 (a), (b) and (c); i.e., 29.72% (Zn) and 70.28% (O), 36.82% (Zn), and 63.18% (O), and 36.08% (Zn), and 63.92% (O) respectively.

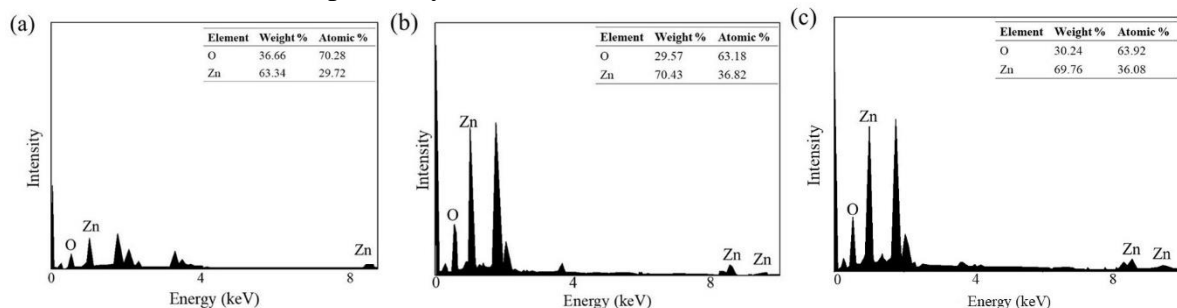


Figure 4: The EDX spectra and elemental analyses (insets) of ZnO thin films fabricated using (a) one, (b) two, and (c) three evaporation cycles

Figure 5 shows the XRD pattern (in the range of 10° - 80°) of the ZnO thin films; revealed a hexagonal (wurtzite) crystal structure. Broad peaks were presented in thin films fabricated using one evaporation cycle (at $2\theta = 35.74^\circ, 40.14^\circ, 41.05^\circ, 53.06^\circ, 69.26^\circ, 71.98^\circ,$ and 74.98° (Figure 5 a)), and two evaporation cycles (at $2\theta = 30.12^\circ, 34.57^\circ, 35.71^\circ, 47.41^\circ, 54.76^\circ, 62.52^\circ, 66.45^\circ,$ and 72.68° (Figure 5 b)); correspond to the (i) [002], [100], [101], [102], [103], [110], [004], and (ii) [100], [002], [101], [102], [110], [103], [201], and [004] crystal planes respectively. Slight difference could be observed at higher angles in the crystal planes of the ZnO thin film deposited using three evaporation cycles i.e., $2\theta = 36.71^\circ, 39.09^\circ, 43.26^\circ, 54.53^\circ, 62.70^\circ, 69.92^\circ,$ and 70.77° [43]; correspond to the [002], [100], [101], [102], [103], [201], [110] crystal planes respectively (Figure 5 c).

The increment of intensity of the diffraction of the crystal planes with increasing number of cycles is clearly observed. The angles of the measured diffraction peaks are consistent; however, the intensity of the peaks increases. The three evaporation cycles-based ZnO thin film is dominated by the ZnO crystals arranged in the direction of [100] crystal plane, as indicated by the highest diffraction intensity; hypothesized would exhibit higher electron mobility than that of the one and two evaporation cycles [46, 47]. This observation could be due to the improvement of crystallinity and small grain size which might facilitate electron transfer in the ZnO and suppress the recombination of electrons [48, 49]. A similar behaviour was observed by Öztaş et al. [50, 51]. Moreover, the cause of difference in the crystal plane of one and two evaporation cycles could be due to intrinsic defect in the ZnO thin film i.e., zinc vacancy [52]. Intrinsic defects are generated due to the presence of impurity in the materials and exposure of samples at higher temperature [52]. The defect could be resulted from the variation of the intrinsic defects in ZnO film, such as (i) zinc vacancy V_{Zn} , (ii) oxygen vacancy V_O , (iii) interstitial zinc Zn_i , (iv) interstitial oxygen O_i , and (v) antisite oxygen O_{Zn} . This observation could be due to the presence of interstitial Zn and oxygen vacancies in the film as confirmed by the results of EDX spectroscopy. In addition, poor crystallinity in thinner ZnO thin films could be due to incomplete crystallization, as only a few atomic layers of disordered atoms constitute the bulk of the film [53]. The results in Figure 5 indicated that the crystallinity and degree of orientation of the ZnO thin films were closely related to the film thickness.

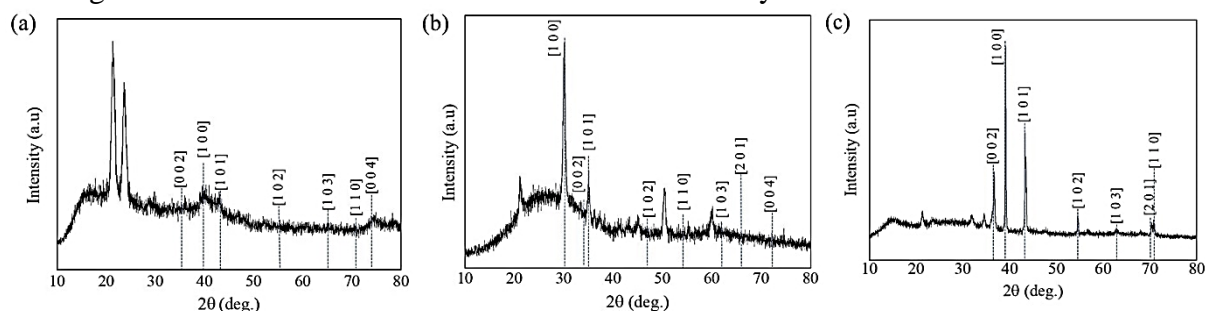


Figure 5: (a) The XRD pattern of ZnO thin films fabricated using (a) one, (b) two, and (c) three evaporation cycles

Morphological Analysis

The morphology of the ZnO thin films was simulated using Shape V7.4 software based on their crystal properties – showed a spherical shape as shown in the inset of Figure 6 a(i), b(i), and c(i); confirmed by FESEM. The diameter of the nanosphere distributions on the

surface of the deposited ZnO thin film using one, two, and three evaporation cycles i.e., ca. 8 – 20 nm, ca. 11 – 37 nm, and ca. 6 – 16 nm respectively (Figure 6). The thickness of the thin films is 92 nm (one evaporation cycle), 411 nm (two evaporation cycles), and 508 nm (three evaporation cycles) respectively (Figure 6 a(ii), b(ii), and c(ii)). It is noticeable from the FESEM images that size distribution decreases from 20 to 16 nm (Figure 7) with an increment of the thickness from 92.12 to 508 nm. The FESEM images of the films with higher thickness indicate that the films are composed of a dense packing of grains without any cracks, indicating good quality of the thin films. It has also been confirmed from the XRD analysis that the intensity of peaks increases with the increase in the thin film thickness which shows the improved crystallinity. The size reduction of the ZnO below its exciton Bohr radius (ca. 1.8 nm) would increase the bandgap due to quantum confinement effect [54].

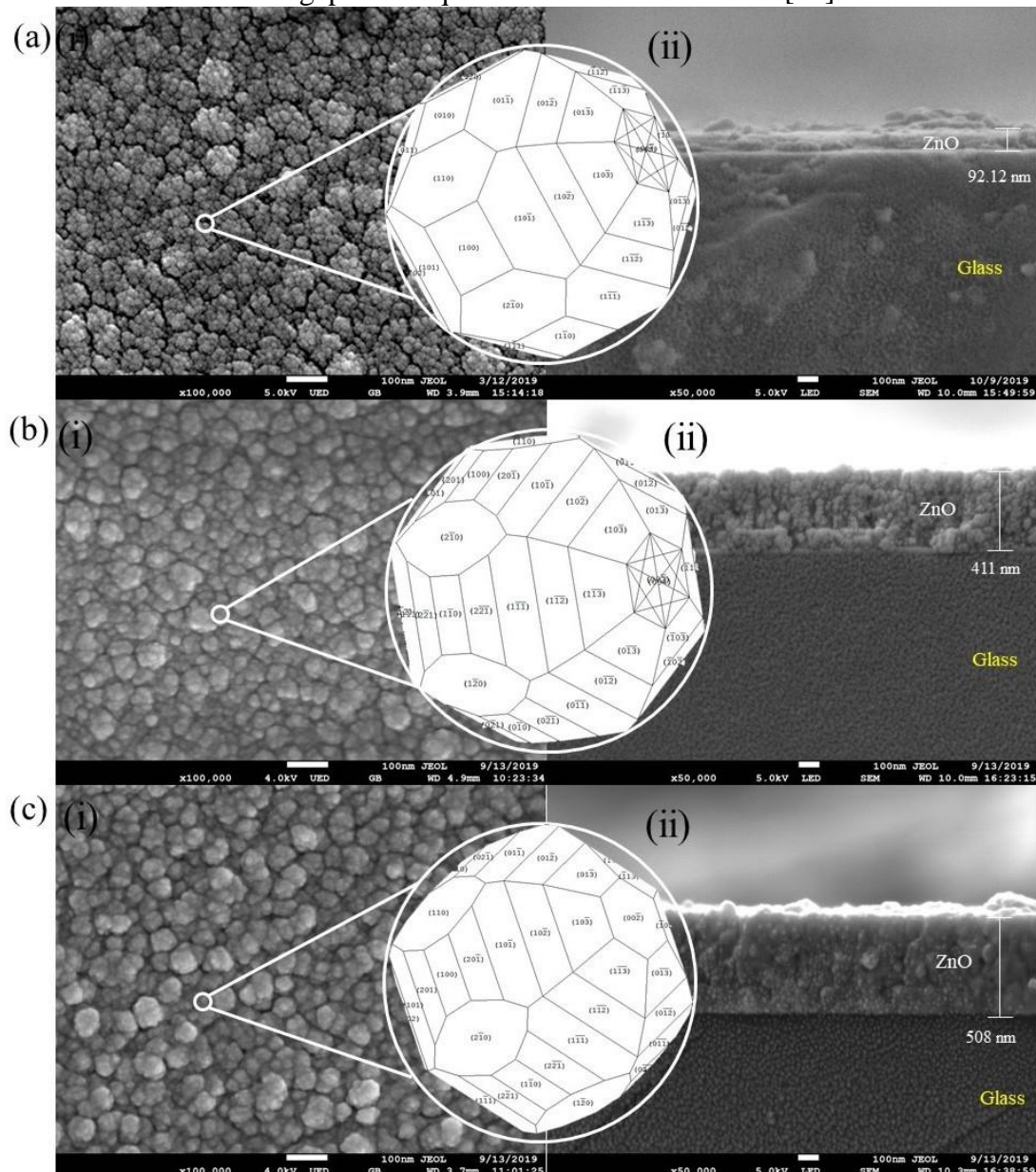


Figure 6: The FESEM micrographs reveal that the ZnO thin films deposited using (a)(i) one, (b)(i) two, and (c)(i) three-evaporation cycles technique consist of small spherical particles. The cross section thin films showed the thickness of (a)(ii) one (92 nm), (b)(ii) two (411 nm), and (c)(ii) three (508 nm) evaporation cycles.

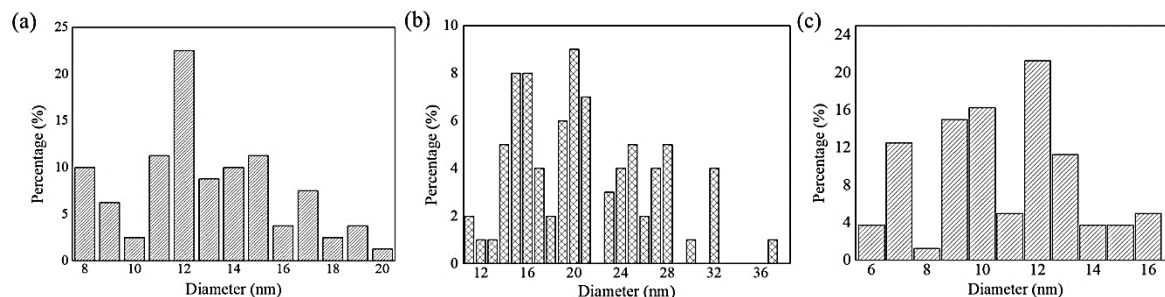


Figure 7. The diameter of the nanosphere distributions of ZnO thin films deposited using (a) one, (b) two, and (c) three- evaporation cycles technique

Optical characterization

The effect of film thickness on the optical properties such as band gap of ZnO thin films was investigated. Absorption spectra of (a) one, (b) two and (c) three evaporation cycles of ZnO are shown in the insets of Figure 8. The spectra were fitted to four Gaussian peaks, revealed four excitonic transitions (in the sequence of first, second, third, and fourth transition) for the ZnO thin films fabricated using one, two, and three evaporation cycles viz., (a) (i) 658.90 nm, (ii) 524.60 nm, (iii) 401.92 nm, and (iv) 274.64 nm, (b) (i) 705.85 nm, (ii) 591.58 nm, (iii) 481.86 nm, and (iv) 346.78 nm, and (c) (i) 715.83 nm, (ii) 593.05 nm, (iii) 458.95 nm, and (iv) 325.89 nm respectively. The position of the first excitonic peak shifted to longer wavelength with increment of evaporation cycles. The observation could be attributed to the small size and narrow size distributions of ZnO fabricated using the three evaporation cycles [55, 56].

The optical bandgap of the films was estimated using Tauc’s plot (Figure 8); using the following equations (1, 2)

$$a = \frac{1}{t} \left(\frac{A}{\log e} \right) \tag{1}$$

$$ahv = A(hv - E_g)^{1/2} \tag{2}$$

where t is the thickness of quartz cell, A is the absorbance of the samples, e is the charge of an electron, h is Planck’s constant, ahv is the energy of photon, and E_g is the bandgap [57-59]. The E_g of the ZnO thin films deposited using one, two, and three evaporation cycles was estimated as 2.40 eV, 2.54 eV, and 2.60 eV respectively.

The increment of the E_g with increasing thickness of the film is accompanied by an enhancement of crystallinity; which could be attributed to decrement of strain in the film [60] and partial reduction of oxygen-ion vacancy [52, 61]. Furthermore, defects i.e., zinc vacancy in the thin films deposited using low number of evaporation cycle would contribute to decrement of crystallinity [62]. In addition, the blue shift of the E_g could be also due to several factors such as grain size, structural parameters and lattice strain, carrier concentration, presence of impurities (or other defects), or even deviation from stoichiometry [63]. Similar

blue shift in E_g values for the films with smaller grain sizes have been reported for electrochemical deposited nanosized ZnO [64].

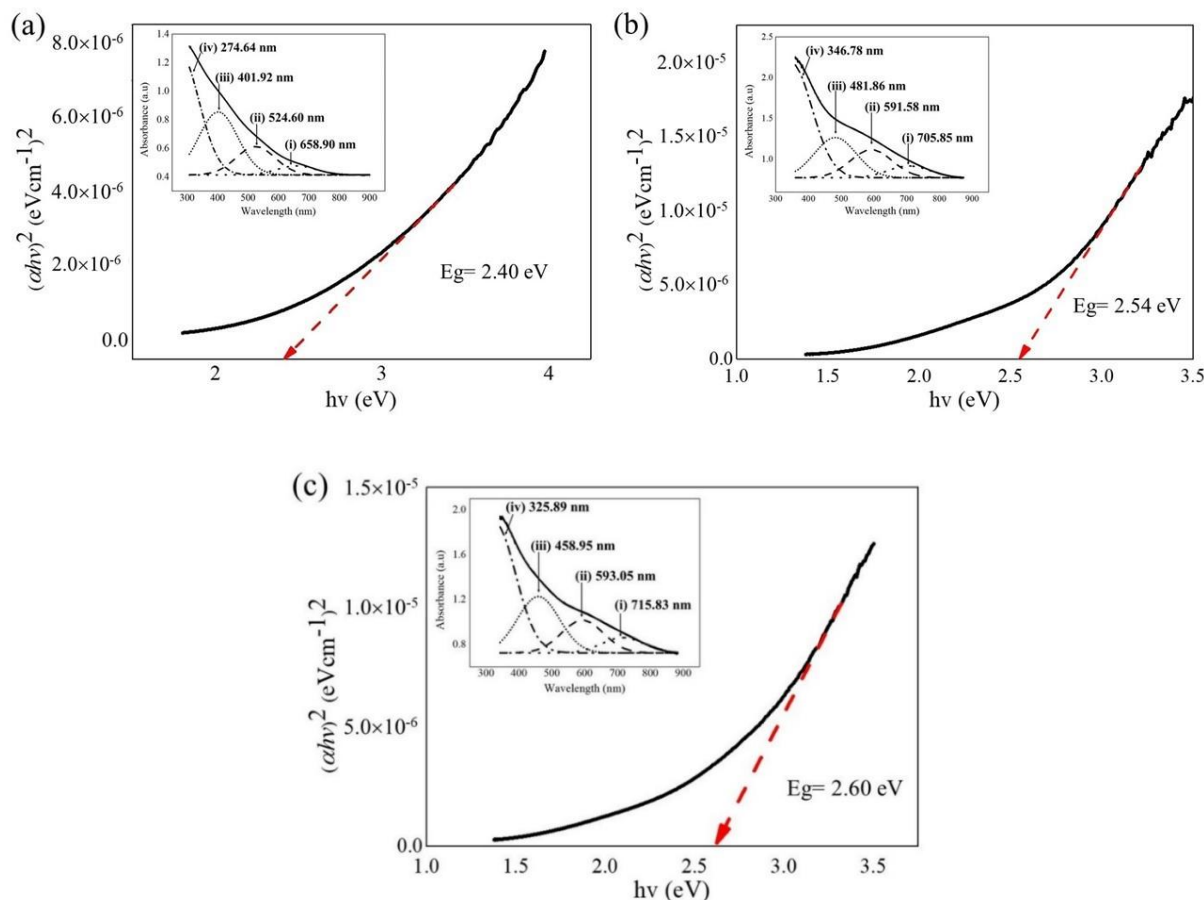


Figure 8: Tauc's plot of the ZnO thin films fabricated using (a) one, (b) two, and (c) three evaporation cycles

Conclusions

In conclusion, a simple approach in deposition of ZnO thin film via thermal evaporation method were successfully demonstrated with different number of evaporation cycle. The ZnO thin films were characterized using EDX, XRD, FESEM and UV-Visible-NIR absorption spectrometer. The results from the EDX and XRD indicate that intrinsic defect which exists in the ZnO thin films deposited using one, and two evaporation cycles technique would exhibit low electron mobility, in comparison with that of the three evaporation cycles.

The absorption spectra show a clear correlation between number of evaporation cycle, thickness of thin film and the E_g . The film thickness would affect the crystallinity due to (i) defect (zinc vacancy), and (ii) strain in the film. Moreover, the morphology analysis revealed that the decrement of range of the size distribution of the nanospheres would also increase the E_g . This observation could be originated from the increment of number of ZnO crystals which are smaller than their exciton Bohr radius (ca. 2.34 nm – non observable by the FESEM) which in the range of strong quantum confinement regime.

Acknowledgement

This work is funded by the Research & Innovation Department of Universiti Malaysia Pahang, and the Ministry of Education of Malaysia through the Fundamental Research Grant Scheme (RDU 150111) and Postgraduate Research Scheme (PGRS1903198).

Author Contributions

All authors contributed towards data analysis, drafting and critically revising the paper and agree to be accountable for all aspects of the work.

Disclosure of Conflict of Interest

The authors have no disclosures to declare.

Compliance with Ethical Standards

The work is compliant with ethical standards.

References

- [1] Suma, M. N., Prasad, M. V. N., Gaddam, V., Rajanna, K., & Nayak, M. (2019). Development of a Novel Acoustic Sensor using Sputtered ZnO Thin Film. *J. Pure Appl. Ind. Phys*, 9, 1-7.
- [2] Saravanan, A., Huang, B. R., & Kathiravan, D. (2018). Bio-industrial Waste Silk Fibroin Protein and Carbon Nanotube-Induced Carbonized Growth of One-Dimensional ZnO-based Bio-nanosheets and their Enhanced Optoelectronic Properties. *Chem. Eur. J.*, 24(48), 12574-12583.
- [3] Li, B., Xi, B., Feng, Z., Lin, Y., Liu, J., Feng, J., & Xiong, S. (2018). Hierarchical porous nanosheets constructed by graphene-coated, interconnected TiO₂ nanoparticles for ultrafast sodium storage. *Adv. Mater.*, 30(10), 1705788.
- [4] Demirci, Ö., Haşimi, N., Kilinc, E., & Tolan, V. (2018). Evaluation of Genotoxic Effects of C60 Fullerene- γ -Fe₂O₃ and Multi-Wall Carbon Nanotubes- γ -Fe₂O₃ Nanoparticles. *Kafkas Univ. Vet. Fak.*, 24(6).
- [5] Liu, J., Gan, H., Wu, H., Zhang, X., Zhang, J., Li, L., & Wang, Z. (2018). Effect of Organic Substrates on the Photocatalytic Reduction of Cr (VI) by Porous Hollow Ga₂O₃ Nanoparticles. *J. Nanomater.*, 8(4), 263.
- [6] Azmi, F. F. A., Sahraoui, B., & Muzakir, S. K. (2019). Study of ZnO nanospheres fabricated via thermal evaporation for solar cell application. *Makara J. Technol.*, 23(1), 11-15.
- [7] Zheng, J., Q. Jiang, and Lian, J. (2011). Synthesis and optical properties of flower-like ZnO nanorods by thermal evaporation method. *Appl. Surf. Sci.*, 257(11), 5083-5087.
- [8] Omri, K., Alyamani, A., & El Mir, L. (2019). Surface morphology, microstructure and electrical properties of Ca-doped ZnO thin films. *J. Mater. Sci.: Mater. Electron.*, 30(17), 16606-16612.

- [9] Malik, G., Mourya, S., Jaiswal, J., & Chandra, R. (2019). Effect of annealing parameters on optoelectronic properties of highly ordered ZnO thin films. *Mater. Sci. Semicond Process*, 100, 200-213.
- [10] Wang, Y., Xu, H., Zan, G., Wu, T., & Wu, Q. (2020). A pie-like structure double-sidedly assembled with ZnO-nanodisks vertically on Cu-nanoplates and its photochemical properties. *Chemosphere*, 127292.
- [11] Lee, H. Y., Lin, T. S., & Lee, C. T. (2018). Stacked WO₃ nanosphere and WO₃ thin film metal-semiconductors-metal ultraviolet photodetectors. *ECS J. Solid State Sci. Technol.*, 7(5), Q85.
- [12] Alsultany, F. H., Majdi, H. S., Abd, H. R., Hassan, Z., & Ahmed, N. M. (2019). Catalytic growth of 1D ZnO nanoneedles on glass substrates through vapor transport. *J. Electron. Mater.*, 48(3), 1660-1668.
- [13] Xu, X., Guo, Y., Liang, Z., Cui, H., & Tian, J. (2019). Remarkable charge separation and photocatalytic efficiency enhancement through TiO₂ (B)/anatase heterophase junctions of TiO₂ nanobelts. *Int. J. Hydrog. Energy*, 44(50), 27311-27318.
- [14] Garoufalis, C. S., Zeng, Z., Bester, G., Hayrapetyan, D. B., & Baskoutas, S. (2019). Optical properties of zig-zag and armchair ZnO colloidal nanoribbons. *Chem. Phys. Lett.*, 732, 136659.
- [15] Wei, Q., Wang, Y., Yin, J., Xia, Y., & Liu, Z. (2019). High-Performance Visible-Light Photodetectors built on 2D-Nanoplate-Assembled Large-Scale BiI₃ Films. *Adv. Electron. Mater.*, 5(7), 1900159.
- [16] Yan, X., Song, Y., Zhu, C., Li, H., Du, D., Su, X., & Lin, Y. (2018). MnO₂ nanosheet-carbon dots sensing platform for sensitive detection of organophosphorus pesticides. *Anal. Chem.*, 90(4), 2618-2624.
- [17] Yao, X., Li, Z., Liu, C., Yang, L., Li, H., Liu, X., ... & Bao, Y. (2019). Ultraviolet nanolaser of inverted hexagonal ZnO pyramid resonating in helical whispering-gallery-like mode. *Opt. Express*, 27(23), 34454-34462.
- [18] Rahman, M. U., Wei, M., Xie, F., & Khan, M. (2019). Efficient dye-sensitized solar cells composed of nanostructural ZnO doped with Ti. *Catalysts*, 9(3), 273.
- [19] Zarezadeh, S., Habibi-Yangjeh, A., & Mousavi, M. (2019). BiOBr and AgBr co-modified ZnO photocatalyst: a novel nanocomposite with p-n heterojunctions for highly effective photocatalytic removal of organic contaminants. *J. Photochem. Photobiol. A*, 379, 11-23.
- [20] Zhang, S., Liu, Z., Ruan, M., Guo, Z., Lei, E., Zhao, W., & Chen, D. (2020). Enhanced piezoelectric-effect-assisted photoelectrochemical performance in ZnO modified with dual cocatalysts. *Appl. Catal. B*, 262, 118279.
- [21] Rana, A. K., Kumar, M., Ban, D. K., Wong, C. P., Yi, J., & Kim, J. (2019). Enhancement in Performance of Transparent p-NiO/n-ZnO Heterojunction Ultrafast Self-Powered Photodetector via Pyro-Phototronic Effect. *Adv. Electron. Mater.*, 5(8), 1900438.
- [22] Luo, J., Dai, X., Bai, S., Jin, Y., Ye, Z., & Guo, X. (2013). Ligand exchange of colloidal ZnO nanocrystals from the high temperature and nonaqueous approach. *Nanomicro Lett.*, 5(4), 274-280.
- [23] Sahal, M., Hartiti, B., Ridah, A., Mollar, M., & Mari, B. (2008). Structural, electrical and optical properties of ZnO thin films deposited by sol-gel method. *Microelectron. Int.*, 39(12), 1425-1428.
- [24] Quintana, M., Edvinsson, T., Hagfeldt, A., & Boschloo, G. (2007). Comparison of dye-sensitized ZnO and TiO₂ solar cells: studies of charge transport and carrier lifetime. *J. Phys. Chem. C*, 111(2), 1035-1041.
- [25] Mia, M. N. H., Pervez, M. F., Hossain, M. K., Rahman, M. R., Uddin, M. J., Al Mashud, M. A., & Hoq, M. (2017). Influence of Mg content on tailoring optical bandgap of Mg-doped ZnO thin film prepared by sol-gel method. *Results Phys.*, 7, 2683-2691.

- [26] Zhu, L., Li, Y., & Zeng, W. (2018). Hydrothermal synthesis of hierarchical flower-like ZnO nanostructure and its enhanced ethanol gas-sensing properties. *Appl. Surf. Sci.*, 427, 281-287.
- [27] Hunge, Y. M., Mahadik, M. A., Moholkar, A. V., & Bhosale, C. H. (2017). Photoelectrocatalytic degradation of phthalic acid using spray deposited stratified WO₃/ZnO thin films under sunlight illumination. *Appl. Surf. Sci.*, 420, 764-772.
- [28] Fan, H., Xu, S., Cao, X., Liu, D., Yin, Y., Hao, H., & Shen, Y. (2017). Ultra-long Zn₂SnO₄-ZnO microwires based gas sensor for hydrogen detection. *Appl. Surf. Sci.*, 400, 440-445.
- [29] Thongsuksai, W., Panomsuwan, G., & Rodchanarowan, A. (2018). Fast and convenient growth of vertically aligned ZnO nanorods via microwave plasma-assisted thermal evaporation. *Mater. Lett.*, 224, 50-53.
- [30] Wisz, G., Virt, I., Sagan, P., Potera, P., & Yavorskyi, R. (2017). Structural, optical and electrical properties of Zinc Oxide layers produced by pulsed laser deposition method. *Nanoscale Res. Lett.*, 12(1), 253.
- [31] Tatebayashi, J., Yoshii, G., Nakajima, T., Kamei, H., Takatsu, J., Lebrun, D. M., & Fujiwara, Y. (2018). Control of the energy transfer between Tm³⁺ and Yb³⁺ ions in Tm, Yb-codoped ZnO grown by sputtering-assisted metalorganic chemical vapor deposition. *J. Appl. Phys.*, 123(16), 161409.
- [32] Bai, S., Wu, Z., Xu, X., Jin, Y., Sun, B., Guo, X., & Han, X. (2012). Inverted organic solar cells based on aqueous processed ZnO interlayers at low temperature. *Appl. Phys. Lett.*, 100(20), 203906.
- [33] Jagadamma, L. K., Abdelsamie, M., El Labban, A., Aresu, E., Ndjawa, G. O. N., Anjum, D. H., ... & Amassian, A. (2014). Efficient inverted bulk-heterojunction solar cells from low-temperature processing of amorphous ZnO buffer layers. *J. Mater. Chem. A*, 2(33), 13321-13331.
- [34] You, J., Chen, C. C., Dou, L., Murase, S., Duan, H. S., Hawks, S. A., & Yang, Y. (2012). Metal oxide nanoparticles as an electron-transport layer in high-performance and stable inverted polymer solar cells. *Adv. Mater.*, 24(38), 5267-5272.
- [35] Manor, A., Katz, E. A., Tromholt, T., & Krebs, F. C. (2012). Enhancing functionality of ZnO hole blocking layer in organic photovoltaics. *Sol. Energy Mater. Sol.*, 98, 491-493.
- [36] Small, C. E., Chen, S., Subbiah, J., Amb, C. M., Tsang, S. W., Lai, T. H., & So, F. (2012). High-efficiency inverted dithienogermole–thienopyrrolodione-based polymer solar cells. *Nat. Photonics*, 6(2), 115-120.
- [37] Guo, Y., Yin, X., Liu, J., Chen, W., Wen, S., Que, M., & Gao, B. (2019). Vacuum thermal-evaporated SnO₂ as uniform electron transport layer and novel management of perovskite intermediates for efficient and stable planar perovskite solar cells. *Org. Electron.*, 65, 207-214.
- [38] Lan, X., Voznyy, O., Kiani, A., García de Arquer, F. P., Abbas, A. S., Kim, G. H., & Yuan, M. (2016). Passivation using molecular halides increases quantum dot solar cell performance. *Adv. Mater.*, 28(2), 299-304.
- [39] Kim, G. H., García de Arquer, F. P., Yoon, Y. J., Lan, X., Liu, M., Voznyy, O., & Hoogland, S. (2015). High-efficiency colloidal quantum dot photovoltaics via robust self-assembled monolayers. *Nano Lett.*, 15(11), 7691-7696.
- [40] Xiao, Y., Han, G., Chang, Y., Zhang, Y., Li, Y., & Li, M. (2015). Investigation of perovskite-sensitized nanoporous titanium dioxide photoanodes with different thicknesses in perovskite solar cells. *J. Power Sources*, 286, 118-123.
- [41] Keis, K., Magnusson, E., Lindström, H., Lindquist, S. E., & Hagfeldt, A. (2002). A 5% efficient photoelectrochemical solar cell based on nanostructured ZnO electrodes. *Sol. Energy Mater. Sol.*, 73(1), 51-58.

- [42] Huang, C. Y., Hsu, Y. C., Chen, J. G., Suryanarayanan, V., Lee, K. M., & Ho, K. C. (2006). The effects of hydrothermal temperature and thickness of TiO₂ film on the performance of a dye-sensitized solar cell. *Sol. Energy Mater Sol.*, 90(15), 2391-2397.
- [43] Shin, I., Seo, H., Son, M. K., Kim, J. K., Prabakar, K., & Kim, H. J. (2010). Analysis of TiO₂ thickness effect on characteristic of a dye-sensitized solar cell by using electrochemical impedance spectroscopy. *Curr. Appl. Phys.*, 10(3), S422-S424.
- [44] Kao, M. C., Chen, H. Z., Young, S. L., Kung, C. Y., & Lin, D. C. (2009). The effects of the thickness of TiO₂ films on the performance of dye-sensitized solar cells. *Thin Solid Films*, 517(17), 5096-5099.
- [45] Chuang, C. H. M., Brown, P. R., Bulović, V., & Bawendi, M. G. (2014). Improved performance and stability in quantum dot solar cells through band alignment engineering. *Nat. Mater.*, 13(8), 796-801.
- [46] Sun, Y., Seo, J. H., Takacs, C. J., Seifert, J., & Heeger, A. J. (2011). Inverted polymer solar cells integrated with a low-temperature-annealed sol-gel-derived ZnO film as an electron transport layer. *Adv. Mater.*, 23(14), 1679-1683.
- [47] Gopikrishnan, R., Zhang, K., Ravichandran, P., Baluchamy, S., Ramesh, V., Biradar, S., & Ramesh, G. T. (2010). Synthesis, characterization and biocompatibility studies of zinc oxide (ZnO) nanorods for biomedical application. *Nanomicro Lett.*, 2(1), 31-36.
- [48] Benkő, G., Skårman, B., Wallenberg, R., Hagfeldt, A., Sundström, V., & Yartsev, A. P. (2003). Particle size and crystallinity dependent electron injection in fluorescein 27-sensitized TiO₂ films. *J. Phys. Chem. B*, 107(6), 1370-1375.
- [49] Chung, J., Lee, J., & Lim, S. (2010). Annealing effects of ZnO nanorods on dye-sensitized solar cell efficiency. *Physica B Condens. Matter*, 405(11), 2593-2598.
- [50] Öztaş, M., Bedir, M., Yazici, A. N., Kafadar, E. V., & Toktamış, H. (2006). Characterization of copper-doped sprayed ZnS thin films. *Physica B Condens. Matter*, 381(1-2), 40-46.
- [51] Öztas, M., & Bedir, M. (2008). Thickness dependence of structural, electrical and optical properties of sprayed ZnO: Cu films. *Thin Solid Films*, 516(8), 1703-1709.
- [52] Agarwal, D. C., Chauhan, R. S., Kumar, A., Kabiraj, D., Singh, F., Khan, S. A., & Satyam, P. V. (2006). Synthesis and characterization of ZnO thin film grown by electron beam evaporation. *J. Appl. Phys.*, 99(12), 123105.
- [53] Kakati, N., Jee, S. H., Kim, S. H., Oh, J. Y., & Yoon, Y. S. (2010). Thickness dependency of sol-gel derived ZnO thin films on gas sensing behaviors. *Thin Solid Films*, 519(1), 494-498.
- [54] Azmi, F. F. A., Kadir, M. F. Z., Aziz, S. B., & Muzakir, S. K. (2020). Characterization of opto-electronic properties of thermally evaporated ZnO. *Mater. Today*, 29, 179-184.
- [55] Tüzemen, E. Ş., Eker, S., Kavak, H., & Esen, R. (2009). Dependence of film thickness on the structural and optical properties of ZnO thin films. *Appl. Surf. Sci.*, 255(12), 6195-6200.
- [56] Talghader, J. J., Gawarikar, A. S., & Shea, R. P. (2012). Spectral selectivity in infrared thermal detection. *Light Sci. Appl.*, 1(8), e24-e24.
- [57] Muzakir, S. K. (2014). Identification of (CdSe)₃₂ structure in microemulsion-based synthesis for solar cell applications. In Malaysia University Conference Engineering Technology.
- [58] Rathore, K. S., Deepika, Patidar, D., Saxena, N. S., & Sharma, K. (2010). Cadmium sulphide nanocrystallites: synthesis, optical and electrical studies. In AIP Conference Proceedings, 1249, (1), 145-148.
- [59] Sönmezoglu, S., Taş, R., Akın, S., & Can, M. (2012). Polyaniline micro-rods based heterojunction solar cell: structural and photovoltaic properties. *Appl. Phys. Lett.*, 101(25), 253301.

- [60] Al-Khawaja, S., Abdallah, B., Abou Shaker, S., & Kakhia, M. (2015). Thickness effect on stress, structural, electrical and sensing properties of (0 0 2) preferentially oriented undoped ZnO thin films. *Compos. Interfaces*, 22(3), 221-231.
- [61] Borah, D. J., Mostako, A. T. T., Saikia, P. K., & Dutta, P. (2019). Effect of thickness and post deposition annealing temperature on the structural and optical properties of thermally evaporated molybdenum oxide films. *Mater. Sci. Semicond. Process*, 93, 111-122.
- [62] Jazmati, A. K., & Abdallah, B. (2018). Optical and structural study of ZnO thin films deposited by RF magnetron sputtering at different thicknesses: a comparison with single crystal. *Mater. Res.*, 21(3).
- [63] Enríquez, J. P., & Mathew, X. (2003). Influence of the thickness on structural, optical and electrical properties of chemical bath deposited CdS thin films. *Sol. Energy Mater Sol.*, 76(3), 313-322.
- [64] Gao, F., Naik, S. P., Sasaki, Y., & Okubo, T. (2006). Preparation and optical property of nanosized ZnO electrochemically deposited in mesoporous silica films. *Thin Solid Films*, 495(1-2), 68-72.